

Article

# Isolating and Quantifying the Effects of Climate and CO<sub>2</sub> Changes (1980–2014) on the Net Primary Productivity in Arid and Semiarid China

Xia Fang <sup>1,2,3,4</sup>, Chi Zhang <sup>1,\*</sup>, Quan Wang <sup>5</sup>, Xi Chen <sup>1</sup>, Jianli Ding <sup>3</sup> and Fidele Karamage <sup>1,2</sup>

<sup>1</sup> State Key Laboratory of Desert and Oasis Ecology, Xinjiang Institute of Ecology and Geography, Chinese Academy of Sciences, Urumqi, Xinjiang 830011, China; newage-sun@163.com (X.F.); chenxi@ms.xjb.ac.cn (X.C.); fidelekaramage@yahoo.com (F.K.)

<sup>2</sup> University of Chinese Academy of Sciences, Beijing 100049, China

<sup>3</sup> School of Resources and Environment, Xinjiang University, Xinjiang 830046, China; ding\_jl@163.com

<sup>4</sup> Xinjiang Polytechnical College, Urumqi, Xinjiang, 830091, China

<sup>5</sup> Faculty of Agriculture, Shizuoka University, Shizuoka 422-8529, Japan; wang.quan@shizuoka.ac.jp

\* Correspondence: zc@ms.xjb.ac.cn; Tel.: +86-991-782-3127

Academic Editor: Timothy A. Martin

Received: 31 December 2016; Accepted: 22 February 2017; Published: 28 February 2017

**Abstract:** Although the net primary productivity (NPP) of arid/semiarid ecosystem is generally thought to be controlled by precipitation, other factors like CO<sub>2</sub> fertilization effect and temperature change may also have important impacts, especially in the cold temperate areas of the northern China, where significant warming was reported in the recent decades. However, the impacts of climate and atmospheric CO<sub>2</sub> changes to the NPP dynamics in the arid and semiarid areas of China (ASA-China) is still unclear, hindering the development of climate adaptation strategy. Based on numeric experiments and factorial analysis, this study isolated and quantified the effects of climate and CO<sub>2</sub> changes between 1980–2014 on ASA-China's NPP, using the Arid Ecosystem Model (AEM) that performed well in predicting ecosystems' responses to climate/CO<sub>2</sub> change according to our evaluation based on 21 field experiments. Our results showed that the annual variation in NPP was dominated by changes in precipitation, which reduced the regional NPP by 10.9 g·C/(m<sup>2</sup>·year). The precipitation-induced loss, however, has been compensated by the CO<sub>2</sub> fertilization effect that increased the regional NPP by 14.9 g·C/(m<sup>2</sup>·year). The CO<sub>2</sub> fertilization effect particularly benefited the extensive croplands in the Northern China Plain, but was weakened in the dry grassland of the central Tibetan Plateau due to suppressed plant activity as induced by a drier climate. Our study showed that the climate change in ASA-China and the ecosystem's responses were highly heterogeneous in space and time. There were complex interactive effects among the climate factors, and different plant functional types (e.g., phreatophyte vs. non-phreatophyte) could have distinct responses to similar climate change. Therefore, effective climate-adaptive strategies should be based on careful analysis of local climate pattern and understanding of the characteristic responses of the dominant species. Particularly, China's policy makers should pay close attention to climate change and ecosystem health in northeastern China, where significant loss in forest NPP has been triggered by drought, and carefully balance the ecological and agricultural water usage. For wildlife conservation, the drought-stressed grassland in the central Tibetan Plateau should be protected from overgrazing in the face of dramatic warming in the 21st century.

**Keywords:** AEM model; net primary productivity (NPP); climate change; CO<sub>2</sub> fertilization effect; arid; semiarid China

## 1. Introduction

Global ecosystem sustainability is threatened by the dramatic rise of atmospheric CO<sub>2</sub> and the accompanying climate changes [1]. An arid and semiarid ecosystem is more sensitive to climate changes than other terrestrial ecosystems [2–6]. It covers 36% of the world's land area and half of China's land [7], and is facing serious threats from climate changes like drought and warming [8]. Climate change in China has been dramatic in recent decades, particularly in the arid and semiarid areas of China (ASA-China), where the temperature has increased at a rate of 0.48 °C/decade (2000–2010) and droughts/floods have threatened ecosystem sustainability [9]. As a key indicator of ecological health, net primary productivity (NPP) has been widely used in investigations of the effects of climate change on ecosystem functions [10–12]. It is necessary to understand the temporal and spatial characteristics of NPP based on various climatic factors in ASA-China in the context of CO<sub>2</sub> effects and climate change. Such knowledge is critical for the development of effective climate adaptation strategies in ASA-China.

Multiple studies have investigated the overall dynamics of terrestrial NPP in China based on remote sensing models [12–16]. However, remote sensing data only reflect the combined effects of all driving factors, including air pollution, land-use change, etc. Additionally, the relative contributions of different factors to NPP dynamics cannot be quantitatively isolated and decomposed [17]. To isolate the climate/CO<sub>2</sub> change effects from other factors like land-use changes, climate control experiments such as the Free-Air Carbon dioxide Enrichment (FACE) are required [18]. NPP dynamics is vital in the study of global carbon balance. Factors and processes that impact NPP dynamics include climate changes and land-use change [19]. Specifically, land-use changes within terrestrial ecosystems on carbon balance are important in global change study, which has triggered tremendous research in recent decades [20].

Although field experiments provide valuable insights about ecosystems' responses to climate change and the underlying controlling mechanisms, they are usually conducted at site level, focusing on a certain ecosystem type, and addressing a limited combination of climate change scenarios. Given the spatial heterogeneity of environment variables (climate, vegetation, soil types, terrains, etc.) in the real world, and the non-linear responses of terrestrial ecosystem to climate changes, it is not appropriate to directly extrapolate the site-level results to regional scale (e.g., in ASA-China). It is also impossible to conduct climate control experiments at the regional scale in field studies. Alternatively, process-based ecosystem models that incorporate knowledge gained through field experiments and have been well-validated against field observations provide a feasible approach to conduct climate control experiments at regional/global scales [21–24]. Well-designed numeric experiments and factorial analyses can isolate the impacts of individual factors and their interactive effect, and reveal the spatial patterns of NPP/carbon dynamics in response to different climate change drivers [25].

In this study, we applied the Arid Ecosystem Model (AEM) [26], a process-based model that has been optimized for the dryland ecosystems in China and Central Asia (see Section 2.2), to isolate and quantify the relative contributions of climate (temperature and precipitation) and CO<sub>2</sub> changes (1980–2014) to the NPP dynamics in ASA-China, and to reveal the spatiotemporal characteristics of the dominant factors (i.e., the climate factor that has the strongest effects on the NPP dynamic in a certain area). To achieve the objectives, we first compiled the reports from field climate/CO<sub>2</sub>-control experiments and used the data to evaluate the performance of AEM in predicting ecosystems' responses to climate/CO<sub>2</sub> changes; then we conducted five numeric experiments over the ASA-China region to simulate the regional NPP dynamics in response to different climate control scenarios; finally, the relative contributions of individual factors and their interactive effects were quantified with a carefully designed factorial analysis scheme. By comparing the strengths of the climate/CO<sub>2</sub> change effects, we developed a map that shows the spatial pattern of dominant factors over the NPP of ASA-China. It should be emphasized that this study only focused on isolating and comparing the impacts of climate/CO<sub>2</sub> changes on NPP, not on assessing the overall NPP dynamic of the real world. The latter is affected by many other factors besides climate and CO<sub>2</sub> (land-use change, air pollution, etc.), which are out of the scope of this study).

## 2. Materials and Methods

### 2.1. Study Area

Arid and semiarid regions of China (27.6°N–53.6°N, 73.4°E–127.5°E) cover an area of  $5.23 \times 10^6$  km<sup>2</sup>, with a complex terrain with altitudes ranging from –152 m to 8563 m (Figure 1) [27]. The study area belongs to the temperate continental climate with low and unevenly distributed precipitation, which generally decreases from southeast to northwest [28]. The study area could be further divided into arid region (precipitation  $\leq 200$  mm/year) and semiarid region (precipitation  $> 200$  mm/year) [29]. The major plant functional types (PFTs) are evergreen needleleaf forest (ENF), broadleaf forest (BDF), phreatophytic shrubland (PS), non-phreatophytic shrubland (NPS), grassland (GRS), cropland (CRP) and meadow (MEW) (Figure 1). We assumed that all cropland was irrigated in the arid/semiarid environment. Non-vegetated areas, including mobile deserts, glaciers, etc., are not considered in this study.

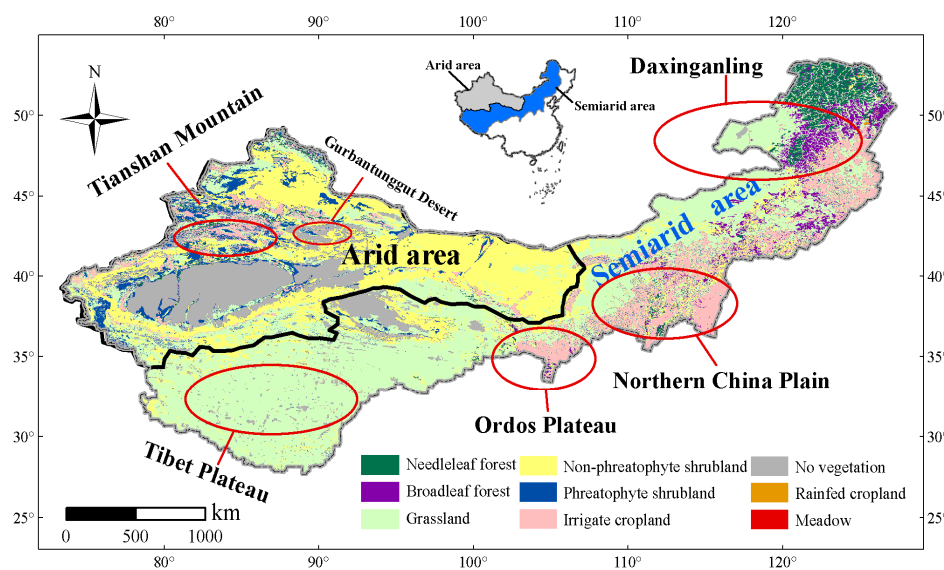


**Figure 1.** Study area and distribution of plant functional types (based on vegetation map of the People's Republic of China (1:1,000,000)) [30].

### 2.2. Arid Ecological Model (AEM)

Based on knowledge gained from field studies on the northern temperate dryland, the AEM is a process-based ecosystem model that couples biophysical processes (energy balance) and biogeochemical processes (carbon and water processes) [26]. It is a spatially explicit model that uses a daily time step to simulate the impacts of climate change on ecosystem processes. Specifically the AEM addresses the structure of dryland vegetation and their energy, carbon and water processes by including an improved vertical root distribution module, a mechanistic module for water movement along the groundwater-soil-root-canopy continuum, and a plant form module that dynamically updates a plant's aboveground structure (tree height, crown size, stem, etc.) on a daily basis. These improvements helped the model to correctly simulate the canopy energy process in sparsely vegetated ecosystems (while the popular "big-leaf" assumption in other models may overestimate the light interception and heat stress of shrub canopy), and soil water movement and uptake (especially groundwater usage) by dryland vegetation. Like most spatial-explicit models, the AEM adopts the concept of PFTs to describe vegetation distribution. The model has been parameterized for the seven major PFTs in ASA-China as shown in Figure 1. Being optimized for the northern temperate dryland, the AEM has been applied in climate change studies in Xinjiang, China [31] and Central Asia [32].

In comparison to other models, the AEM does not use a heuristic approach to approximate the effects of soil water stress on stomatal conductance. The stomatal conductance is related to photosynthesis, which is controlled by the leaf-absorbed PAR, ambient CO<sub>2</sub> concentration, and environmental factors such as temperature. The AEM estimates the C assimilation rate of a plant following a biochemical model of leaf photosynthesis originally developed by Farquhar [33] and subsequently expanded by Collatz [34] and other researchers [35,36].

Leaf photosynthesis is the minimum of RuBP carboxylase's (Rubisco) limited rate of carboxylation ( $w_c$ ), the light-limited rate of carboxylation ( $w_j$ ), and the export limited rate of carboxylation ( $w_e$ ). For C<sub>4</sub> PFT,  $w_e$  refers to the PEP carboxylase limited rate of carboxylation [33].

$$A = \min(w_c, w_j, w_e)$$

$$w_c = \begin{cases} \frac{(c_i - \Gamma_*) \times V_{max}}{c_i + K_c \times (1 + \frac{o_2}{K_o})} & (C_3 \text{ PFT}) \\ V_{max} & (C_4 \text{ PFT}) \end{cases}$$

$$w_j = \begin{cases} \frac{(c_i - \Gamma_*) \times 4.6 \times \alpha \times Rad_{abs,PAR}}{c_i + 2 \times \Gamma_*} & (C_3 \text{ PFT}) \\ 4.6 \times \alpha \times Rad_{abs,PAR} & (C_4 \text{ PFT}) \end{cases} \quad (1)$$

$$w_e = \begin{cases} 0.5 \times V_{max} & (C_3 \text{ PFT}) \\ 4000 \times V_{max} \frac{c_i}{P_{pressure}} & (C_4 \text{ PFT}) \end{cases}$$

where  $c_i$  and  $o_i$  are the partial pressure of internal leaf CO<sub>2</sub> and O<sub>2</sub>, respectively (Pa);  $P_{pressure}$  is the atmospheric pressure (Pa);  $K_c$  and  $K_o$  are the Michaelis-Menten constants for CO<sub>2</sub> and O<sub>2</sub>, 30 ranging from three to four for different PFTs, respectively [26];  $\Gamma_*$  is the CO<sub>2</sub> compensation point (Pa), ranging from 1.7 to 2.2 for different PFTs [26]; absorbed PAR ( $Rad_{abs,PAR}$ ) is converted to photosynthetic photon flux by assuming 4.6  $\mu$ mol photons per joule;  $\alpha$  is the quantum efficiency, ranging from 0.056 to 0.07 [26];  $V_{max}$  is the maximum rate of carboxylation varied with temperature (T, °C), and the water potential of the crown ( $\psi_{crn}$ , kPa):

$$V_{max} = V_{max25} \times \alpha_{vmax}^{\frac{T-25}{10}} \times f(T) \times f(\psi_{crn}) \quad (2)$$

where  $V_{max25}$  is the maximum carboxylation rate at 25 °C;  $\alpha_{vmax}$  is a temperature sensitivity parameter, indicating the magnitude of change in  $V_{max}$  with temperature altering every 10 °C away from the reference temperature (25 °C);  $f(T)$  is an empirical function that delineates the response of leaf carboxylation to temperature;  $f(\psi_{crn})$  is an empirical function that delineates the response of leaf carboxylation to the leaf water potential.

$$f(T) = \left[ 1 + \exp\left(\frac{-220000 + 710(T + 273.16)}{8.314(T + 273.16)}\right) \right]^{-1} \quad (3)$$

$$f(\psi_{crn}) = \min\left\{1, \max\left[0, \frac{(\psi_{crn} - \psi_{close})}{(\psi_{open} - \psi_{close})}\right]\right\} \quad (4)$$

where  $\psi_{close}$  and  $\psi_{open}$  are thresholds of crown water potential (kPa) at which stomata of leaf begin to fully close and fully open respectively;  $\psi_{crn}$  is calculated as

$$\psi_{crn} = \sum_{n=1}^N (Rootfract_n \times \psi_n) + 15 \times H \quad (5)$$

where  $n$  denotes the  $n$ th soil layer;  $\psi_n$  (kPa) denotes the water potential in soil layer  $n$ ;  $Rootfract_n$  denotes the fraction of root biomass in soil layer  $n$ ;  $H$  (m) is the height of plant.  $H = 0$  for non-woody plants. Following Friend [37], AEM assumes that the effective water potential decreases by 15 kPa/meter from soil surface to the top of crown.

Currently, AEM does not consider the impacts of nitrogen limitation on ecosystem productivity. Considering the high N deposition rate in China [38], nitrogen-limitation effect on China's ecosystems may not be strong. Nevertheless, this limitation brings uncertainty to this study.

The sink term (S) in Richard's equation, i.e., the rate of root water uptake, is determined by two factors: the water demanded by the plants to support potential transpiration ( $P_{tran}$ , mm/day) and the maximum water uptake capacity of the root system under the current soil moisture condition ( $Wup_{max}$ , mm/day).

$$S = tran = \min(p_{tran}, Wup_{max})$$

$$Wu_{max} = \sum_{n=1}^N Wu_{p_{max},n}$$
(6)

The AEM estimates  $Wup_{max}$ , using a mechanistic submodel that considers both the radial and axial liquidflow in the rhizosphere and through the lateral and tape root. Considering a 1D steadystate flow in a series network, the liquid flow equation is

$$Wup_n = \frac{h_{rt,n} - h_0}{r_{xt,n}} = \frac{h_{lr,n} - h_{rt,n}}{r_{xl}} = \frac{h_{rz,n} - h_{lr,n}}{r_{rz,n}} = \frac{h_{rz,n} - h_b}{r_{xt,n} + r_{xl} + r_{rz,n}}$$
(7)

where  $h_b$ ,  $h_{tr,n}$ ,  $h_{lr,n}$ , and  $h_{rz,n}$  (mm) are the water pressure heads at the stem base, tape root xylem, lateral root xylem, and rhizosphere (in soil layer n), respectively;  $r_{xt,n}$  and  $r_{xl}$  (days) are the axial resistance to water flow in the tape root and lateral root xylems respectively; and  $r_{rz,n}$  (day) is the resistance to the water flow that passes through the rhizosphere and enters the fine root [26].

### 2.3. Model Validation

Model validation and evaluation are the processes of assessing the accuracy and consistency of simulation results relative to measured data [39]. In previous studies, the performance of AEM has been evaluated by sensitivity analyses and validations against field observations, including daily evapotranspiration, NPP, vegetation biomass and soil carbon storage at several long-term research sites and more than 350 field plots in northwestern China and Central Asia [31,32]. Although all of the PFTs in this study (Figure 1) have been included in the previous model validations, we conducted additional model evaluation against reported NPP in the semiarid ecosystems of northeastern China and the Tibetan Plateau (Table 1).

**Table 1.** List of field-observed net primary productivity (NPP) for model validation.

Location	Longitude	Latitude	Dominant PFT	Year	NPP (g C/(m <sup>2</sup> ·year))	Methodology	Source
Tianshui	105.75	34.58	Broadleaf forest	1960–2011	608.00	Model estimated	Jiang et al. [40]
Xilin Gole	116.63	43.72	Grassland	1980–1989	248.63	Field observations	[41]
Changbai	121.5	50.83	Broadleaf forest	1960–2014	594.66	Model estimated	Wu et al. [42]
Bole	82.73	44.84	Phreatophytic shrub	1997–2006	422.73	Field observations	Wang et al. [43]
Zhaosu	81.12	43.23	Needleleaf forest	1941–2002	529.50	Field observations	Su et al. [44]
Yiwu	93.95	43.42	Needleleaf forest	1981–2001	188.50	Field observations	Su et al. [44]
Tianchi	88.11	43.89	Needleleaf forest	1900–2000	539.00	Field observations	Su et al. [44]
Xiaoquzi	87.11	43.48	Needleleaf forest	1929–2002	547.00	Field observations	Su et al. [44]
Bange	89.98	31.67	Alpine steppe	2001	67.49	Field observations	Pei et al. [45]
Tianzhu	102.43	37.2	Grassland	1980–1981	536.75	MODIS-retrieved	Wang et al. [46]

Furthermore, we evaluated the AEM performance in predicting ecosystems' responses to changes in temperature, precipitation, and CO<sub>2</sub>. This task is particularly important because it is directly related to the objective of this study. Only after the AEM successfully replicates the observed ecosystem responses to climate/CO<sub>2</sub> changes from field studies, can we have confidence in its capacity to correctly predict the NPP dynamic across large areas in climate-control (numeric) experiments. Otherwise, any numeric experiments can only be treated as sensitivity analyses of the model. For this purpose, we compiled reports of climate-control studies from 21 field experiment sites (Table 2), and compared the model predictions against observations (Figure 2c–e). Although this study aims to investigate the

responses of NPP to CO<sub>2</sub>/climate change, many of the field experiments only reported the biomass observations (Table 2). For these validation sites, we calculated the C/A ratios of the model-simulated biomass changes and compared the results against field observations. We assumed that if AEM can correctly simulate biomass response to climate change, it can also correctly simulate the response of NPP.

**Table 2.** List of climate-control experiments for model evaluation in terms of the climate and atmospheric CO<sub>2</sub> effects on NPP. DBF: deciduous broadleaf forest; ENF: evergreen needleleaf forest; GRS: grassland; SRB: shrubland.

PFT	Validation Sites	Experiments Descriptions	Field-Observed Data	References
ENF	USDA Forest Service Institute of Forest Genetics (Placerville, CA, USA)	Ambient CO <sub>2</sub> : 352 ppm, Elevated CO <sub>2</sub> : 700 ppm	Biomass	Walker et al. [47]
ENF	Piedmont Area in North Carolina	Ambient CO <sub>2</sub> : 350 ppm, Elevated CO <sub>2</sub> : 650 ppm.	Biomass	Thomas et al. [48]
ENF	Southeastern France (Ventoux)	Ambient CO <sub>2</sub> : 350 ppm, Elevated CO <sub>2</sub> : 800 ppm.	Biomass	Kaushal et al. [49]
ENF	31°41'07"N, 103°53'58"E	Warming (2.2 ± 0.2 °C)	Biomass	Yang et al. [50]
DBF	Harvard Forest, Petersham, Massachusetts	Ambient CO <sub>2</sub> : 400 ppm, Elevated CO <sub>2</sub> : 700 ppm.	Biomass	Bazzaz et al. [51]
DBF	29°10'19.4"N–29°17'41.4"N, 18°03'49.7"E–118°11'12.2"E	Precipitation enrichment: +30%	Biomass	Yan et al. [52]
GRS	The Great Basin Desert of North America	Ambient CO <sub>2</sub> : 340 ppm, Elevated CO <sub>2</sub> : 680 ppm.	NPP	Smith et al. [53]
GRS	IHR-Littlehampton, UK	Ambient CO <sub>2</sub> : 360 ppm, Elevated CO <sub>2</sub> : 720 ppm.	Biomass	Hunt et al. [54]
GRS	Changling grassland ecological site, Heilongjiang, China	Ambient CO <sub>2</sub> : 350 ppm, Elevated CO <sub>2</sub> : 700 ppm.	Biomass	Gao [55]
GRS	Haibei alpine meadow ecological research site, China	Warming: +1 °C	Biomass	Zhou et al. [56]
GRS	123°44'E–123°47'E, 44°40'N–44°44'N	Warming: +1.7 °C	Biomass	Gao et al. [57]
GRS	37°29'N–37°45' N, 101°12'E–101°23'E	Warming: +(1.15–1.87) °C	Biomass	Li et al. [58]
GRS	Fenghuo Mountainous research site, Tibet, China	Warming: +2 °C	Biomass	Li et al. [59]
GRS	37°29'N–37°45'N, 101°12'E–101°33'E	Precipitation enrichment: +20%	Biomass	Wang et al. [60]
SRB	Nevada Desert FACE Facility at southern Nevada, USA	Ambient CO <sub>2</sub> : 380 ppm, Elevated CO <sub>2</sub> : 550 ppm.	NPP	Housman et al. [61]
SRB	Southwestern United States	Ambient CO <sub>2</sub> : 390 ppm, Elevated CO <sub>2</sub> : 710 ppm.	Biomass	Polley et al. [62]
SRB	The University of Arizona Maricopa Agricultural Center	Ambient CO <sub>2</sub> : 370 ppm, Elevated CO <sub>2</sub> : 550 ppm.	NPP	Mauney et al. [63]
SRB	43°33'N, 142°53'E	Warming: +1.5 °C	NPP	Kudo et al. [64]
SRB	Institute of Botany, C.A.S 116°17'E, 39°57'N	Warming: +3 °C	Biomass	Xiao et al. [65]
SRB	Dengkou, Inner Mongolia and Min Qin, Gansu, China	Warming: +50%	Biomass	Zhu et al. [66]
SRB	112°40'25"E, 42°46'52"N	Warming: +40%	Biomass	Chang [67]

#### 2.4. Model Input Data for the Arid and Semiarid (ASA)-China Simulation

The simulations were conducted with a daily time-step with a spatial resolution of 50 km × 50 km. The daily climate data are derived from NASA's MERRA meteorological reanalysis dataset (1/2° × 2/3°), including precipitation (mm/day), relative humidity (%), shortwave radiation (W·m<sup>-2</sup>), maximum temperature (°C), average temperature (°C) and minimum temperature (°C). Other input datasets include (1) the topographic maps (elevation, slope, and aspects) derived from the 30 m resolution ASTER (the Advanced Space-borne Thermal Emission and Reflection Radiometer) Global Digital Elevation Model Version 2 dataset (ASTER GDEM, v2, Industry (METI) of Japan and the United States National Aeronautics and Space Administration (NASA)) (2) the 1 km resolution soil maps (bulk density, volumetric content of sand and clay, and pH) based on the HWSO (Harmonized World Soil Database) version 1.2 global soil dataset, (3) the annual atmospheric CO<sub>2</sub> concentrations from 1979 to 2014 according to the Mauna Loa observations, and (4) the PFT map derived from the vegetation map of China [30]. All input datasets were aggregated or resampled (bilinear interpolation) to 50 km × 50 km. It should be noted that Figure 1 only shows the dominant PFT (the PFT with the largest coverage) in the study area. In the simulations, a 50 km × 50 km grid (the simulation unit) in the study area could be shared by multiple PFTs, whose relative coverage in the grid were estimated

based on the 1 km resolution vegetation map of China. Each PFT in a grid was simulated separately. The mean NPP of a grid was the area-weighted NPPs of all PFTs that shared the grid.

### 2.5. Numeric Experiments Design and Factorial Analysis

To establish a baseline for the biomass, soil carbon and water pools, the model was run to an equilibrium state with initial climate datasets and CO<sub>2</sub> concentrations of 1980. Because daily climate maps before 1980 are not available for the study region, the climate mean during the first decade of the study period (i.e., 1980–1989) was used to constrain the equilibrium simulation. Then, a spin-up run of 1500 (150 spins × 10 years/spin) was set up to prevent any abnormal fluctuations due to the sudden switch from the equilibration state to the transient state. To match the initial climate conditions for the equilibrium run, each spin was driven by a ten-year detrended climate dataset based on the climate data from 1980 to 1989. After initialization, we applied the time series data for climate and CO<sub>2</sub> to simulate the NPP dynamics.

In order to isolate the effects of individual factor (precipitation, temperature, CO<sub>2</sub> concentration) to the NPP change in the ASA-China, five numeric experiments (or scenarios) were designed (Table 2): The OVERALL scenario stands for the combined effects of climate and CO<sub>2</sub> changes. The CO<sub>2</sub> scenario is a single-factor control experiment in which only the atmospheric CO<sub>2</sub> concentration was allowed to change from year to year, while the other climate factors remained constant (maintaining equilibrium). The output of the CO<sub>2</sub> scenario indicated the impacts of CO<sub>2</sub> change from 1980–2014 on NPP in ASA-China. Similarly, the TEMP scenario and PREC scenarios are single-factor control experiments for the impacts of temperature change and precipitation change, respectively. The CLIM scenario simulated the combination effects of temperature and precipitation. The change in NPP from 1980–2014 was calculated by comparing the mean NPP during the 1997–2014 period and the mean NPP from 1980–1997. Therefore, we designed the following factorial analyses to quantify the individual effects of climate/CO<sub>2</sub> factors and their interactive effects on NPP:

$$\begin{aligned}
 \text{PREC effect} &= \text{NPP}_{1997-2014\_PREC} - \text{NPP}_{1980-1997\_PREC} \\
 \text{TEMP effect} &= \text{NPP}_{1997-2014\_TEMP} - \text{NPP}_{1980-1997\_TEMP} \\
 \text{CLIM effects} &= \text{NPP}_{1997-2014\_CLIM} - \text{NPP}_{1980-1997\_CLIM} \\
 \text{OVERALL effects} &= \text{NPP}_{1997-2014\_OVERALL} - \text{NPP}_{1980-1997\_OVERALL} \\
 \text{TEMP} \leftrightarrow \text{PREC} &= \text{CLIM effect} - \text{TEMP effect} - \text{PREC effect} \\
 \text{CO}_2 \leftrightarrow \text{CLIM} &= \text{OVERALL effect} - \text{CLIM effect} - \text{CO}_2 \text{ effect}
 \end{aligned} \tag{8}$$

where TEMP ↔ PREC is the interactive effect between temperature change and precipitation change; CO<sub>2</sub> ↔ CLIM is the interactive effect between CO<sub>2</sub> change and climate change. The first item in the subscription of NPP denotes the time period (e.g., 1997–2014 indicates the mean NPP from 1997–2014), the second item in the subscription denotes the numeric experiments (Table 1).

## 3. Results

### 3.1. Model Validation/Evaluation

Our simulation results are highly consistent with the reports from other studies, most of which were based on field observations (Table 2) (linear correlation coefficient  $R^2 = 0.86$ , slope = 0.95, RMSE = 72.71) (Figure 2a). In fact, on these ecological research sites where land-use change were small, the performance of AEM exceeded the MODIS (Moderate Resolution Imaging Spectroradiometer) NPP product (MOD 17A3), which seemed to significantly underestimated the dryland NPP in ASA-China (slope = 0.60,  $R^2 = 0.31$ ; RMSE = 210.79) (Figure 2b).

The results showed that the model is able to replicate the observed climate/CO<sub>2</sub> effects across various PFTs in ASA-China. All AEM-simulated NPP values are found to be significantly correlated to observations/measurements ( $p$ -value < 0.01).  $R^2$  and RMSE of the simulated NPP for precipitation and CO<sub>2</sub> manipulation studied are high ( $R^2 > 0.82$ , RSME < 0.07) (Figure 2d,e); while the simulated

NPP at warming experimental sites were relatively low ( $R^2 = 0.47$  and  $RMSE = 0.20$ ) (Figure 2c). In fact, field experiments indicated relatively high uncertainties in warming effects on ecosystem NPP, probably because warming could enhance both photosynthesis rate and water stress (by enhancing evapotranspiration) in temperate ecosystems. This can explain why the responses of dry shrubs to warming are so unpredictable (Figure 2c).

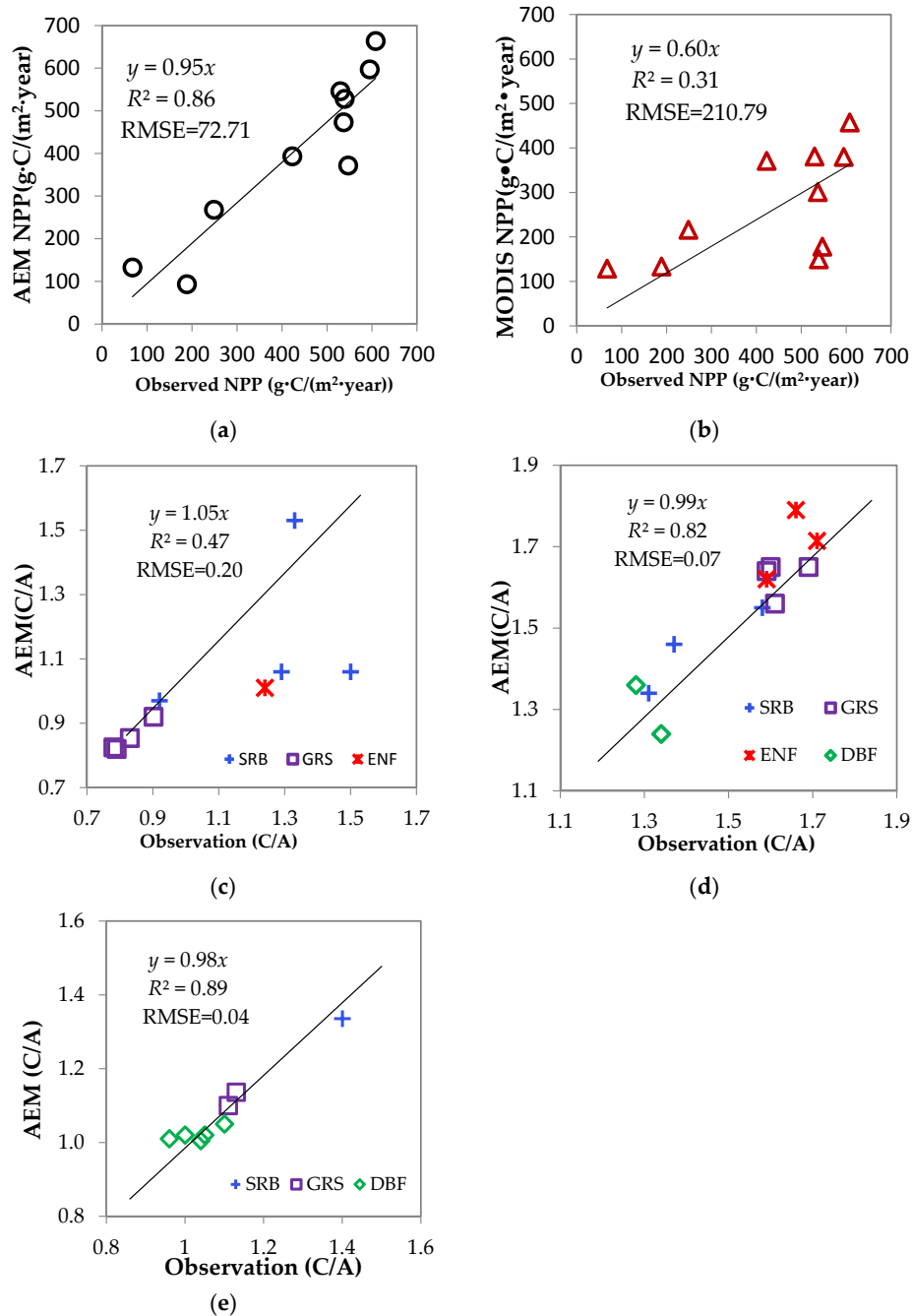


**Figure 2.** Additional model validation: comparing the net primary productivity (NPP) predicted by Arid Ecosystem Model (AEM) (a) and Moderate Resolution Imaging Spectroradiometer (MODIS) data against the field observations in the semiarid ecosystems of ASA-China (b), and evaluating AEM's performance in predicting the responses of plant functional types (PFTs) to changes in temperature (c), atmospheric CO<sub>2</sub> (d), and precipitation (e). The PFTs' responses (C/A) are quantified as the ratios between the NPP under climate/CO<sub>2</sub> change treatments (C) and the NPP under ambient climate/CO<sub>2</sub> (A). GRS: grassland; SRB: shrubland; ENF: evergreen needleleaf forest; DBF: deciduous broadleaf forest.

### 3.2. Spatiotemporal Patterns of Climate Change in Arid and Semiarid Areas of China from 1980–2014

During the 1980–2014 time period, the temperature in the study area had an increasing trend of  $0.2\text{ }^{\circ}\text{C}/10\text{ year}$ ; the annual precipitation decreased by  $0.24\text{ mm/year}$  (Figure 3a); the atmospheric  $\text{CO}_2$  concentration increased  $60\text{ ppmv}$  (Figure 3b). Most (85%) of the study area experienced over  $0.1\text{ }^{\circ}\text{C}$  temperature increase (Figure 3c). Strong warming was found in the Daxinganling area ( $+1.2\text{ }^{\circ}\text{C}$ ) and the central Tibetan Plateau ( $+0.6\text{ }^{\circ}\text{C}$ ). These areas also experienced significant reduction in precipitation (Figure 3d). The annual precipitation in the Ordos Plateau and the mountainous area of Xinjiang increased remarkably ( $>100\text{ mm}$ ).

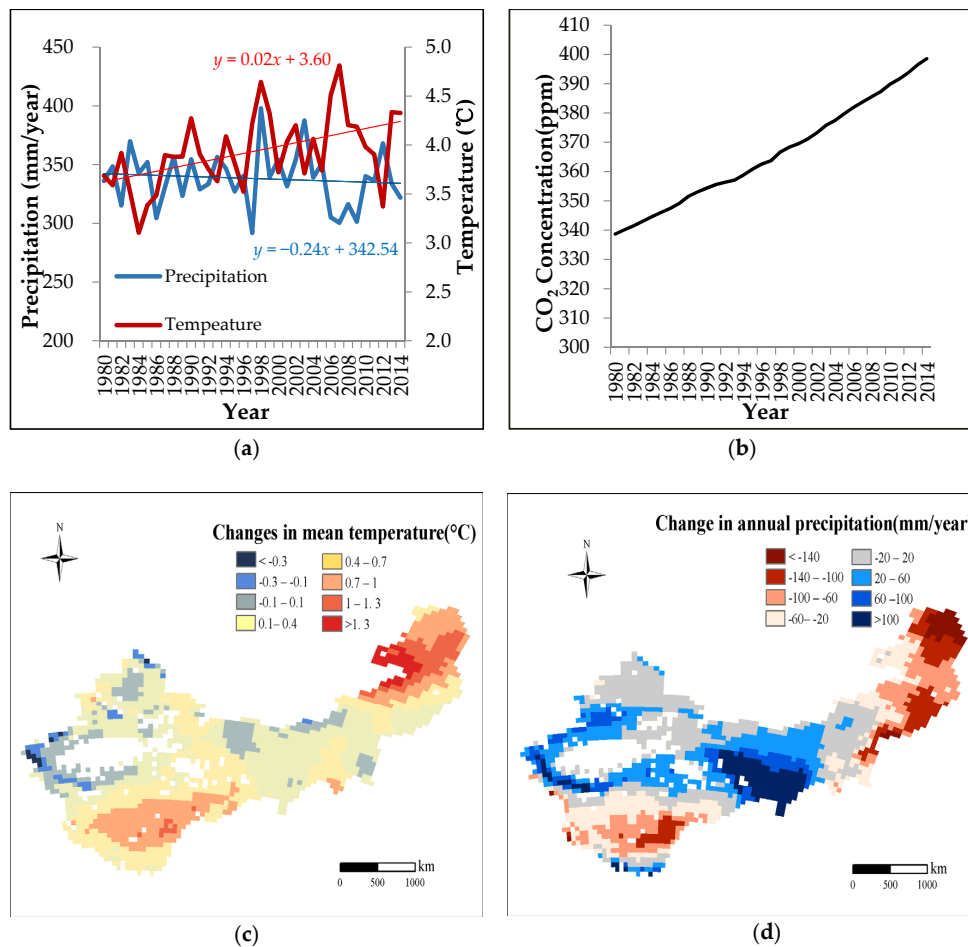


**Figure 3.** The temporal patterns of (a) climate factors and (b)  $\text{CO}_2$  and the spatial patterns of the changes (calculated by subtracting the averages from 1980–1997 from the averages from 1997–2014) in (c) temperature and (d) annual precipitation from 1980 to 2014 in ASA-China.

### 3.3. Impacts of Climate/ $\text{CO}_2$ Changes on Net Primary Productivity (NPP)

The AEM does not use a heuristic approach to approximate the effects of  $\text{CO}_2$  on stomatal conductance and photosynthesis. Instead, AEM estimates the carbon assimilation rate of a plant following a complex biochemical model of leaf photosynthesis originally developed by Farquhar [33] and other researchers [31,32]. In the model, the photosynthesis is co-limited by multiple environmental drivers, including  $\text{CO}_2$ , soil water stress, and temperature, producing a complex NPP dynamic pattern in response to climate/ $\text{CO}_2$  changes similar to that was found in real world. In response to the combined effects of climate and  $\text{CO}_2$  changes (the OVERALL scenario) from 1980–2014, the NPP in ASA-China fluctuated from year to year, significantly correlated with annual precipitation ( $r = 0.71$ ,  $p$ -value  $< 0.05$ ) but not with temperature (Figures 3 and 4). In years with high precipitation, such as

1990, 1994, and 1998, NPP was high; whilst in drought years, such as 1982, 1986, and 1997, NPP was low, indicating strong control from precipitation on the regional NPP dynamic. However, the precipitation change (the PREC scenario) led to an NPP reduction of  $-11 \text{ g}\cdot\text{C}/(\text{m}^2\cdot\text{year})$ , while the OVERALL scenario predicted a slight increase of NPP ( $3 \text{ g}\cdot\text{C}/(\text{m}^2\cdot\text{year})$ ) from 1980–2014, by comparing the mean NPP between 1997–2014 and 1980–1997 (Equation (2)). This was mainly due to the compensation from the  $\text{CO}_2$  fertilization effect (the  $\text{CO}_2$  scenario), which enhanced the NPP by  $15 \text{ g}\cdot\text{C}/(\text{m}^2\cdot\text{year})$ . Because of the  $\text{CO}_2$  compensation effect, the NPP under the OVERALL scenario gradually departed from that under the CLIM scenario in the second half of the study period (Figure 4, Table 3). It is clear that the inter-annual variation of NPP was controlled by climate factors, particularly the precipitation change, but  $\text{CO}_2$  played an important role in determining the long-term trend of NPP in ASA-China (Figure 4). Although most of the ASA-China area experienced warming in the past 35 years (Figure 3c), the effect of temperature change (TEMP effect) was relatively small ( $0.42 \text{ g}\cdot\text{C}/(\text{m}^2\cdot\text{year})$ ) at regional scale (Table 4; Figure 5). The combined effect of climate and  $\text{CO}_2$  changes (the OVERALL effect) was found to be smaller than the sum of CLIM effect and  $\text{CO}_2$  effect, indicating the effects of climate change and  $\text{CO}_2$  change were not additive, and there was a small positive interactive effect ( $0.24 \text{ g}\cdot\text{C}/(\text{m}^2\cdot\text{year})$ ) between the two drivers (Table 4; Figure 5).

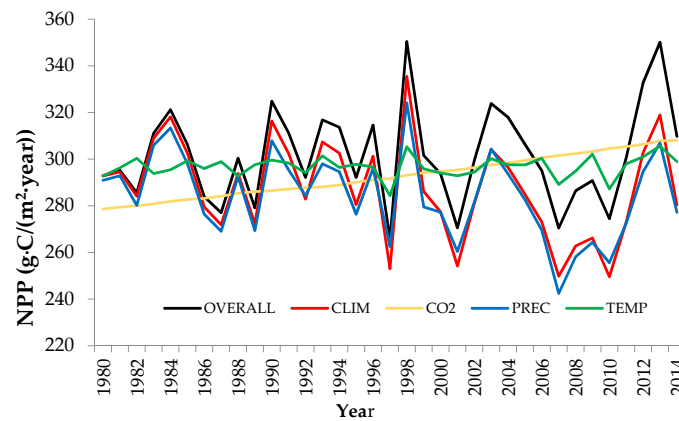


Figure 4. Dynamics of annual NPP under different scenarios (Table 3).

Table 3. Experiment/scenario design.

Scenario	Climate Factors			$\text{CO}_2$	Scenario Description
	Precipitation	Temperature <sup>a</sup>	Other <sup>a</sup>		
OVERALL	1980–2014	1980–2014	1980–2014	1980–2014	Combined effects
$\text{CO}_2$	Equilibrium <sup>b</sup>	Equilibrium	Equilibrium	1980–2014	$\text{CO}_2$ fertilization effect
CLIM	1980–2014	1980–2014	1980–2014	1980	Climate effects
PREC	1980–2014	Equilibrium	Equilibrium	1980	Precipitation effect
TEMP	Equilibrium	1980–2014	Equilibrium	1980	Temperature effect

<sup>a</sup> Temperature refers to the maximum temperature, minimum temperature and average temperature; <sup>b</sup> Equilibrium is the mean climate state of the 1980s.

Table 4. Results of factorial analysis.

Effects	Equations	Data	Results
OVERALL	$\text{NPP}_{1997-2014\_OVERALL} - \text{NPP}_{1980-1997\_OVERALL}$	302.24–299.1	3.14
$\text{CO}_2$	$\text{NPP}_{1997-2014\_CO_2} - \text{NPP}_{1980-1997\_CO_2}$	300.05–285.19	14.86
PREC	$\text{NPP}_{1997-2014\_PREC} - \text{NPP}_{1980-1997\_PREC}$	278.18–289.1	-10.92
TEMP	$\text{NPP}_{1997-2014\_TEMP} - \text{NPP}_{1980-1997\_TEMP}$	296.64–296.22	0.42
CLIM	$\text{NPP}_{1997-2014\_CLIM} - \text{NPP}_{1980-1997\_CLIM}$	282.13–292.48	-10.35
TEMP ↔ PREC	CLIM effect – TEMP effect – PREC effect	-10.35–0.42–(-10.92)	0.15
$\text{CO}_2$ ↔ CLIM	OVERALL effect – CLIM effect – $\text{CO}_2$ effect	3.14–(-10.35)–14.86	-1.37

Table 4 shows the results of our factorial analysis, illustrating the effects of different factors on the annual NPP dynamic ( $\text{g}\cdot\text{C}/(\text{m}^2\cdot\text{year})$ ) by comparing the mean NPP of the first half of the study period (1980–1997) to that of the second half of the study period (1997–2014).

The NPP of all PFTs were stimulated by the elevated  $\text{CO}_2$ . However, different PFT responded very differently to climate change (Figure 5). The effects of precipitation on forests' NPP were most significant. This is partly because the forests (especially the evergreen needleleaf forest) in ASA-China endured strong precipitation decline during the study period, partly because the magnitude of forests' NPP is much larger than that of the grasslands and shrubs. The phreatophytic shrubs are not sensitive to the precipitation change, because they can maintain stable water supply from the groundwater. In contrast, the NPP of non-phreatophytic shrubs was stimulated significantly by the increased precipitation. For the same reason, the irrigated croplands were not very sensitive to the large decline in precipitation.

The spatial pattern is complex. The changes in climate and  $\text{CO}_2$  from 1980–2014 enhanced NPP in northern China (especially the Ordos Plateau where NPP increased over  $100 \text{ g}\cdot\text{C}/(\text{m}^2\cdot\text{year})$ ) and the mountainous areas in the northwest (especially the Tianshan mountain where NPP increased over  $50 \text{ g}\cdot\text{C}/(\text{m}^2\cdot\text{year})$ ), but reduced the NPP in the northeast (esp., the Daxinanling region where NPP was reduced over  $200 \text{ g}\cdot\text{C}/(\text{m}^2\cdot\text{year})$ ) and the central Tibetan Plateau where NPP was reduced over  $100 \text{ g}\cdot\text{C}/(\text{m}^2\cdot\text{year})$ ) (Figure 6a). During the study period, the Ordos Plateau and Tianshan Mountain experienced considerable increase in annual precipitation ( $>80 \text{ mm}/\text{year}$ ) and moderate warming (Figure 3c,d) both of which has positive effects on ecosystem productivity (Figure 6c,d). In contrast, the Daxinanling region and the central Tibetan Plateau faced severe drought (precipitation reduced over  $100 \text{ mm}/\text{year}$ ) and strong warming ( $>1 \text{ }^\circ\text{C}$  in the Daxinanling region), both of which inhibited NPP, particularly in the Daxinanling region (Figure 6c,d). Interestingly, we found negative interactive effects between the  $\text{CO}_2$  and climate change effects in the central Tibetan Plateau (Figure 6e) and negative interactive effect between the temperature and precipitation change effects in the Daxinanling region (Figure 6f).

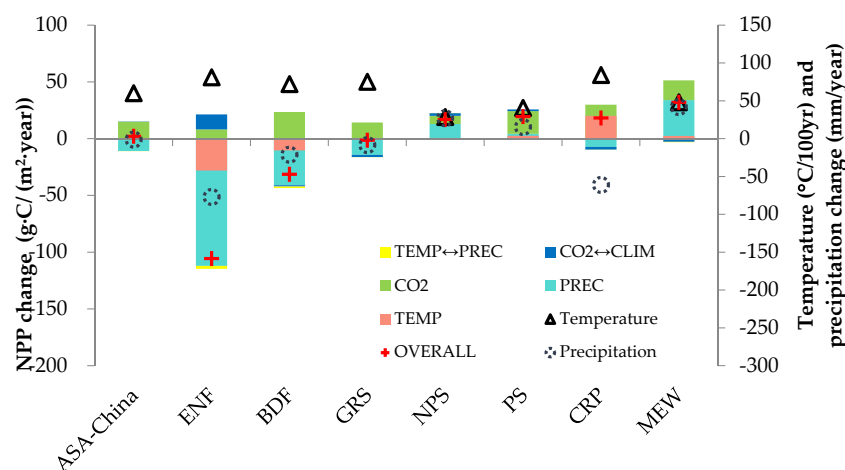


**Figure 5.** Different climate/ $\text{CO}_2$  change effects on the NPP of ASA-China and the major PFTs.  $\text{CO}_2$ :  $\text{CO}_2$  change effect; TEMP: temperature change effect; PREC: precipitation change effect; TEMP ↔ PREC: interactive effect between TEMP and PREC;  $\text{CO}_2$  ↔ CLIM: interactive effect between  $\text{CO}_2$  and climate changes; OVERALL: the overall effects of all climate and  $\text{CO}_2$  changes. Major PFTs: evergreen needleleaf forest (ENF), broadleaf forest (BDF), phreatophytic shrubland (PS), non-phreatophytic shrubland (NPS), grassland (GRS), cropland (CRP) and meadow (MEW). “Temperature” shows the mean temperature change (by comparing the mean temperature during the 1980–1997 period and that of 1997–2014) in the analysis region (e.g., the areas where a certain PFT is distributed); similarly, “Precipitation” shows the mean precipitation change in the analysis region.

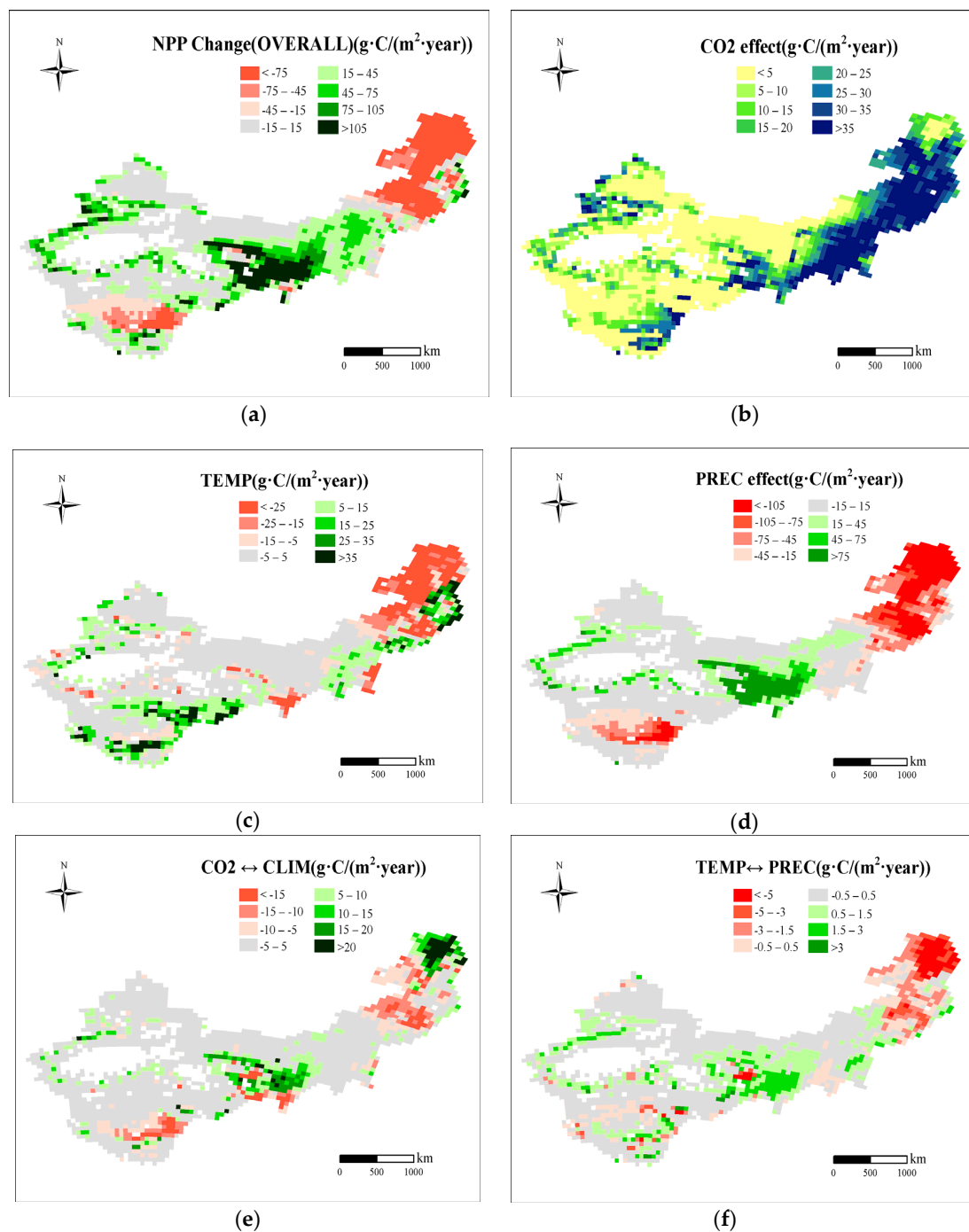


**Figure 6.** Spatial patterns of the NPP change (by comparing the mean NPP during the 1980–1997 period and 1997–2014) in response to changes in climate and CO<sub>2</sub> (a), and the contributions of the CO<sub>2</sub> fertilization effect (b), temperature change effect (c), precipitation change effect (d), and the interactive effects between CO<sub>2</sub> and climate changes (e) and between temperature and precipitation changes (f) to the NPP dynamics in ASA-China, from 1980–2014.

By comparing the effects of different factors, we identified the dominant factor that had the largest impact on NPP (i.e., by comparing the changes in NPP under the influence of each factor) during the past 35 years in each 50 km × 50 km grid in the study area, and developed a map that reveals the dominant climate controls over the NPP in ASA-China (Figure 7). Our study shows that 46% of NPP dynamics in ASA-China were dominated by precipitation changes, especially in northeastern

Daxinganling and northwestern China; CO<sub>2</sub> effect dominated 22% of the region, especially the North China Plain, eastern Inner Mongolia and northwestern desert oases and mountains; about 18% of the region was mainly affected by temperature change, especially in the northeast and southwest of the Tibetan Plateau.

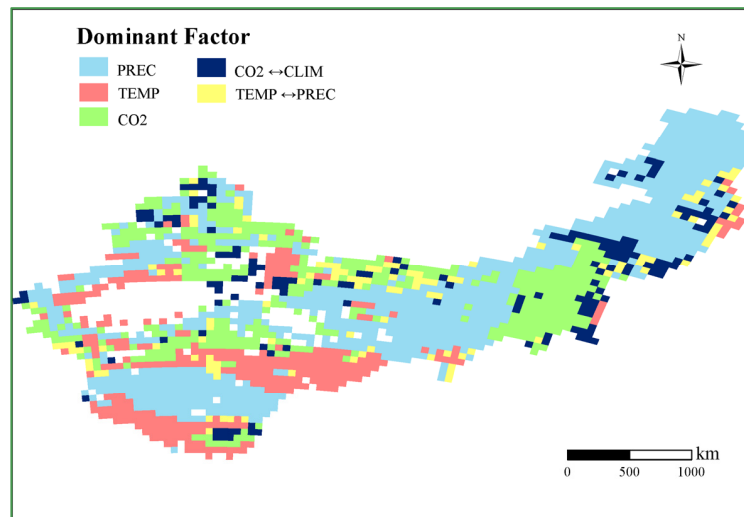


**Figure 7.** The spatial distribution of the dominant factor that controlled the NPP dynamic in ASA-China.

#### 4. Discussion

The anthropogenic changes in climate and atmospheric CO<sub>2</sub> could have important impacts on the sustainability of earth ecosystems and food security [1]. In comparison to land-use change, it is difficult for local governments to reverse or intervene the trend of climate change. Therefore, it is critical to assess the climate change effects and conduct adaptive ecosystem management accordingly. However, quantifying ecosystems' responses to climate change is difficult because of the heterogeneous spatiotemporal pattern in climate factors (Figure 3c,d) and because of the distinct responses from different PFTs (Figures 2b–d and 5). Although field or satellite observations could reveal the overall ecosystem response to global change, it is very difficult to isolate the climate change effects from other local factors like land-use change and air pollution. Some remote sensing studies have used correlation analysis to evaluate the relative importance of different climate factors on ecosystem productivity (e.g., [68]). This approach, however, can neither achieve cause-and-effect inference nor precisely quantify the effect of individual factors. Such objectives can only be achieved by control experiments. Because cost and security issues prohibit field control experiments at the regional scale and ecosystem complexity makes it inappropriate to directly extrapolate the site-level experimental results to regional scale, numeric experiments using mechanistic models is the most cost-effective approach to extrapolate our knowledge gain in field experiments across a large area, providing that these models can correctly reflect ecosystems' responses to climate and CO<sub>2</sub> change [69,70]. In this study, the AEM model has been carefully validated against NPP observations from ten additional sites (Table 1) and findings from 21 field control experiments (Table 2), which gave us confidence that the model can correctly predict the responses of major PFTs in ASA-China to climate and CO<sub>2</sub> changes (Figure 2). The simulation results provided valuable information for climate adaptive management in ASA-China:

Firstly, it showed that the adverse climate change effect (e.g., drought) can be compensated by the CO<sub>2</sub> fertilization effect on NPP in ASA-China. Elevated CO<sub>2</sub> can disrupt the energy balance of the earth system, and may lead to dramatic climate change in some areas and resulting in NPP loss. On the other hand, the CO<sub>2</sub> fertilization effect also typically stimulates plant growth, and might have more important impacts on global ecosystems in the future [71,72]. We found strong CO<sub>2</sub> fertilization effects in most semiarid areas in eastern China, except for the Daxinanling region that experienced severe

precipitation reduction (Figure 6b). Particularly, farmlands in northern China were not sensitive to climate change but were dominated by the CO<sub>2</sub> fertilization effect because of the intensive agricultural management (Figure 7) [47]. This indicates that the food production of China may benefit from the elevated CO<sub>2</sub> in the future as far as there will be no significant degradation of irrigation systems and dramatic decline in precipitation. However, food security in China may be threatened by the severe air/water/soil pollution which is not included in this analysis [73].

Secondly, we suggest China's policy makers pay close attention to climate change and ecosystem health in northeastern China, where the largest forest resources of the nation are located. According to our study, this area experienced significant decrease in precipitation and strong warming in the past 35 years. These climate changes not only had detrimental effects on forest NPP, but could also release large amounts of CO<sub>2</sub> from the carbon-rich soil by stimulating organic matter decomposition. Under an increasingly drier and warmer climate, water supply to the forest ecosystem will become more important. Furthermore, facing an increased water demand from rapidly expanded paddy fields, the local policy makers should carefully balance the agricultural and ecological water usages to maintain sustainable development [74,75].

Thirdly, we should also pay attention to the ecosystem sustainability of the Tibetan Plateau, where the largest protected area of the nation is located (World Database on Protected Areas: [www.Protectedplanet.net](http://www.Protectedplanet.net)). Drought and fast warming in the past 35 years (Figure 3d) could have enhanced water stresses and reduced ecosystem NPP in the central Tibetan Plateau (Figure 6a,d). Projections from 30 CMIP5 (phase five of the Coupled Model Intercomparison Project) models under the Representative Concentration Pathway 4.5 (RCP4.5) scenario indicated the current trend will continue into the 21st century [76]. Compared to 1986–2005, the temperature in 2016–2035 is projected to increase 1.7 °C, while the precipitation may decrease or remain unchanged in most parts of the central Tibetan Plateau. In the face of possible drying in the future, measures should be taken to reduce the stresses on grasslands from overgrazing and the wildlife water holes from the domestic animals.

Besides spatial extrapolation, the factorial analysis based on the AEM simulations also helped us gain insight into the complex interactions among multiple controlling factors. For example, we find a negative interactive effect between the CO<sub>2</sub> and climate factors (i.e., CO<sub>2</sub> ↔ CLIM) in the dry grassland of the central Tibetan Plateau but a strong positive CO<sub>2</sub> ↔ CLIM effect in the Daxinanling region (Figure 6e), although the two regions experienced similar climate change (drought and warming; Figure 3c,d) over the past 35 years. The two regions mainly differed in plant functional types and the background climate regimes. The Daxinanling was occupied by evergreen forest that grew under a relatively humid (annual precipitation > 500 mm/year) [77] climate. Elevated atmospheric CO<sub>2</sub> can reduce the stomatal conductance of the leaf and greatly benefit the forest productivity during drought periods, thus resulting in a strong positive CO<sub>2</sub> ↔ CLIM effect. Elevated CO<sub>2</sub> could also reduce stomatal conductance of the dry grassland in the Tibetan Plateau. However, the background climate in central Tibetan Plateau is drier (annual precipitation < 100 mm/year) [78] than that in northeastern China, and the grassland ecosystem is prevailed by ephemerals and annuals [30] which will shed leaves and enter dormancy during droughts, and thus be irresponsive. When facing drought, the ephemerals and annuals in the grassland will shed leaves and enter dormant, thus be irresponsive to the CO<sub>2</sub> fertilization effect [79]. In other words, the declining precipitation of the past 35 years may have also inhibited the grassland's response to CO<sub>2</sub> in the central Tibetan Plateau.

Even under the same climate regime, different PFT could show distinct responses to similar climate change. For example, in the Gurbantunggut Desert of northwestern China, the increased precipitation has stimulated the NPP of the non-phreatophytic shrubs (e.g., *H. persicum*, *Anabasis*, *Artemisia*, etc.) but had no significant impacts on the phreatophytic shrubs (e.g., the *Tamarix* species) or irrigated crops (Figure 5) [80]. These complex climate interaction effects and plant response pattern indicate that there is no universal rule of thumb to estimate climate change impacts. Effective management strategies should be based on careful analysis of local climate change patterns and understanding of the characteristic responses of the dominant PFT. To this end, our maps show NPP dynamics in response

to various climate controls (Figure 6) and the dominant controlling factor on the NPP in ASA-China (Figure 7) can help policy makers to identify the hotspot of ecosystem degradation/recovery and understand the controlling mechanisms (Figure 7).

## 5. Conclusions

Facing rapid climate change in the recent decades, it is important to assess the impacts of climate factors on ecosystem net primary productivity (NPP) in arid and semiarid (ASA)-China. The Arid Ecosystem Model (AEM) model, which has been validated against field observations, provided us a valuable tool to isolate and quantify the effects of climate and CO<sub>2</sub> changes on the region's NPP over the past 35 years. Our results showed that the annual variations on NPP were dominated by changes in precipitation, which reduced the regional NPP by 10.92 g·C/(m<sup>2</sup>·year). The precipitation change effect, however, was compensated by the CO<sub>2</sub> fertilization effect that increased NPP by 14.86 g·C/(m<sup>2</sup>·year). The CO<sub>2</sub> fertilization effect particularly benefited the large amount of croplands in the Northern China Plain, but was weakened in the dry grassland of the central Tibetan Plateau because of the negative interactive effects between precipitation and the CO<sub>2</sub> effects. The complex climate interaction and plant response patterns revealed by this study indicate that there is no universal rule of thumb to estimate climate change impacts. Effective management strategies should be based on careful analysis of the local climate change pattern and understanding of the characteristic responses of the dominant plant functional types (PFT) to climate/CO<sub>2</sub> changes. Our study results can help policy makers identify hotspots of climate change and the ecosystems that may be most at risk from a drying climate. Particularly, China's policy makers should pay close attention to the climate change and ecosystem health in northeastern China, where significant reduction in forest NPP has been experienced during droughts. In the face of current drought stress and projected fast warming in the 21st century, measures should be taken to preserve the stressed grassland in the central Tibetan Plateau to support the wildlife in this largest protected area of China.

**Acknowledgments:** We thank the editor and the anonymous reviewers for their valuable comments and advice that helped us improve this manuscript. This study was supported by the National Basic Research Programs of China (#2014CB954204) and the International Cooperation and Exchanges of the National Science Foundation of China (# 41361140361).

**Author Contributions:** C.Z. supervised this study. X.F. ran the model and wrote the manuscript. Q.W., X.C., J.D. and F.K. participated in discussion.

**Conflicts of Interest:** The authors declare no conflict of interest.

## References

1. Gray, V. Climate change 2007: The physical science basis. Summary for policy makers. *Energy Environ.* **2007**, *54*, 44–45.
2. Shen, W.; Reynolds, J.F.; Hui, D. Responses of dryland soil respiration and soil carbon pool size to abrupt vs. Gradual and individual vs. Combined changes in soil temperature, precipitation, and atmospheric [CO<sub>2</sub>]: A simulation analysis. *Glob. Chang. Biol.* **2009**, *15*, 2274–2294. [[CrossRef](#)]
3. Chen, F.-H.; Chen, J.-H.; Holmes, J.; Boomer, I.; Austin, P.; Gates, J.B.; Wang, N.-L.; Brooks, S.J.; Zhang, J.-W. Moisture changes over the last millennium in arid central Asia: A review, synthesis and comparison with monsoon region. *Quat. Sci. Rev.* **2010**, *29*, 1055–1068. [[CrossRef](#)]
4. Dai, A. Drought under global warming: A review. *Wiley Interdiscip. Rev. Clim. Chang.* **2011**, *2*, 45–65. [[CrossRef](#)]
5. Shi, Y.; Shen, Y.; Li, D.; Zhang, G.; Ding, Y.; Hu, R.; Kang, E. Discussion on the present climate change from warm-dry to warm-wet in northwest china. *Quat. Sci.* **2003**, *23*, 152–164.
6. Feng, Z.-D.; An, C.; Wang, H. Holocene climatic and environmental changes in the arid and semi-arid areas of China: A review. *Holocene* **2006**, *16*, 119–130. [[CrossRef](#)]
7. Yang, X.; Williams, M. Landforms and processes in arid and semi-arid environments. *Catena* **2015**, *134*, 1–3. [[CrossRef](#)]

8. Li, X.; Liu, X.; Ma, Z. Analysis on the drought characteristics in the main arid regions in the world since recent hundred-odd years. *Arid Zone Res.* **2004**, *21*, 97–103.
9. Wang, H.; Liu, G.; Li, Z.; Ye, X.; Wang, M.; Gong, L. Impacts of climate change on net primary productivity in arid and semiarid regions of China. *Chin. Geogr. Sci.* **2016**, *26*, 35–47. [[CrossRef](#)]
10. Cramer, W.; Bondeau, A.; Woodward, F.I.; Prentice, I.C.; Betts, R.A.; Brovkin, V.; Cox, P.M.; Fisher, V.; Foley, J.A.; Friend, A.D. Global response of terrestrial ecosystem structure and function to CO<sub>2</sub> and climate change: Results from six dynamic global vegetation models. *Glob. Chang. Biol.* **2001**, *7*, 357–373. [[CrossRef](#)]
11. Cao, M.; Prince, S.D.; Li, K.; Tao, B.; SMALL, J.; Shao, X. Response of terrestrial carbon uptake to climate interannual variability in China. *Glob. Chang. Biol.* **2003**, *9*, 536–546. [[CrossRef](#)]
12. Piao, S.; Fang, J.; Zhou, L.; Zhu, B.; Tan, K.; Tao, S. Changes in vegetation net primary productivity from 1982 to 1999 in China. *Glob. Biogeochem. Cycles* **2005**, *19*. [[CrossRef](#)]
13. Lu, L.; Li, X.; Veroustraete, F. Terrestrial net primary productivity and its spatial-temporal variability in western China. *Acta Ecol. Sin.* **2005**, *25*, 1026–1032.
14. Wang, L.-J.; Niu, Z.; Kuang, D. An analysis of the terrestrial npp from 2002 to 2006 in China based on modis data. *Remote Sens. Land Resour.* **2010**, *25*, 113–116.
15. Piao, S.; Yin, G.; Tan, J.; Cheng, L.; Huang, M.; Li, Y.; Liu, R.; Mao, J.; Myneni, R.B.; Peng, S.; et al. Detection and attribution of vegetation greening trend in China over the last 30 years. *Glob. Chang. Biol.* **2015**, *21*, 1601–1609. [[CrossRef](#)] [[PubMed](#)]
16. Pan, J.; Zhen, L.I. Temporal spatial change of vegetation net primary productivity in the arid region of northwest china during 2001 and 2012. *Chin. J. Ecol.* **2015**, *34*, 3333–3340.
17. Li, C.F.; Luo, G.P.; Li, J.L. Net primary productivity and actual evapotranspiration of central Asia in recent 20 years. *Arid Land Geogr.* **2012**, *35*, 919–927.
18. John, A.G.; Scullion, J.; Ostle, N.; Levy, P.E.; Gwynn-Jones, D. Completing the FACE of elevated CO<sub>2</sub> research. *Environ. Int.* **2014**, *73*, 252–258.
19. Houghton, R.; Hackler, J. Sources and sinks of carbon from land-use change in China. *Glob. Biogeochem. Cycles* **2003**, *17*. [[CrossRef](#)]
20. Lai, L.; Huang, X.; Yang, H.; Chuai, X.; Zhang, M.; Zhong, T.; Chen, Z.; Chen, Y.; Wang, X.; Thompson, J.R. Carbon emissions from land-use change and management in China between 1990 and 2010. *Sci. Adv.* **2016**, *2*, e1601063. [[CrossRef](#)] [[PubMed](#)]
21. Bo, T.; Cao, M.K.; Li, K.R.; Gu, F.X.; Ji, J.J.; Mei, H.; Zhang, L.M. Spatial patterns of terrestrial net ecosystem productivity in China during 1981–2000. *Sci. China* **2007**, *50*, 745–753.
22. Zhang, C.; Tian, H.; Pan, S.; Liu, M.; Lockaby, G.; Schilling, E.B.; Stanturf, J. Effects of forest regrowth and urbanization on ecosystem carbon storage in a rural-urban gradient in the southeastern United States. *Ecosystems* **2007**, *11*, 1211–1222. [[CrossRef](#)]
23. Zhang, C.; Li, C.; Chen, X.; Luo, G.; Li, L.; Li, X.; Yan, Y.; Shao, H. A spatial-explicit dynamic vegetation model that couples carbon, water, and nitrogen processes for arid and semiarid ecosystems. *J. Arid Land* **2012**, *5*, 102–117. [[CrossRef](#)]
24. Ren, W.; Tian, H.; Tao, B.; Huang, Y.; Pan, S. China's crop productivity and soil carbon storage as influenced by multifactor global change. *Glob. Chang. Biol.* **2012**, *18*, 2945–2957. [[CrossRef](#)] [[PubMed](#)]
25. Tian, H.; Melillo, J.M.; Kicklighter, D.W.; Pan, S.; Liu, J.; Mcguire, A.D.; Iii, B.M. Regional carbon dynamics in monsoon asia and its implications for the global carbon cycle. *Glob. Planet. Chang.* **2003**, *37*, 201–217. [[CrossRef](#)]
26. Zhang, C.; Li, C.; Luo, G.; Chen, X. Modeling plant structure and its impacts on carbon and water cycles of the central Asian arid ecosystem in the context of climate change. *Ecol. Model.* **2013**, *267*, 158–179. [[CrossRef](#)]
27. Zheng, C.; Wang, Q. Spatiotemporal variations of reference evapotranspiration in recent five decades in the arid land of Northwestern China. *Hydrol. Process.* **2014**, *28*, 6124–6134. [[CrossRef](#)]
28. Lu, J.; Ji, J. A simulation and mechanism analysis of long-term variations at land surface over arid/semi-arid area in north China. *J. Geophys. Res. Atmos.* **2006**, *111*, 1513–1528. [[CrossRef](#)]
29. Jin, J.; Wang, Q.; Li, L. Long-term oscillation of drought conditions in the western China: An analysis of PDSI on a decadal scale. *J. Arid Land* **2016**, *8*, 819–831. [[CrossRef](#)]
30. Zhang, X.; Sun, S.; Yong, S.; Zhou, Z.; Wang, R. *Vegetation Map of the People'S Republic of China (1: 1000000)*; Geological Publishing House: Beijing, China, 2007.

31. Li, C.; Zhang, C.; Luo, G.; Chen, X. Modeling the carbon dynamics of the dryland ecosystems in Xinjiang, China from 1981 to 2007—The spatiotemporal patterns and climate controls. *Ecol. Model.* **2013**, *267*, 148–157. [[CrossRef](#)]
32. Li, C.; Zhang, C.; Luo, G.; Chen, X.; Maisupova, B.; Madaminov, A.A.; Han, Q.; Djenbaev, B.M. Carbon stock and its responses to climate change in central Asia. *Glob. Chang. Biol.* **2015**, *21*, 1951–1967. [[CrossRef](#)] [[PubMed](#)]
33. Farquhar, G.V.; Caemmerer, S.V.; Berry, J. A biochemical model of photosynthetic CO<sub>2</sub> assimilation in leaves of C<sub>3</sub> species. *Planta* **1980**, *149*, 78–90. [[CrossRef](#)] [[PubMed](#)]
34. Collatz, G.J.; Ribas-Carbo, M.; Berry, J. Coupled photosynthesis-stomatal conductance model for leaves of C<sub>4</sub> plants. *Funct. Plant Biol.* **1992**, *19*, 519–538.
35. Sellers, P.; Randall, D.; Collatz, G.; Berry, J.; Field, C.; Dazlich, D.; Zhang, C.; Collelo, G.; Bounoua, L. A revised land surface parameterization (sib2) for atmospheric gcms. Part I: Model formulation. *J. Clim.* **1996**, *9*, 676–705. [[CrossRef](#)]
36. Bonan, G.B. *A Land Surface Model (Lsm Version 1.0) for Ecological, Hydrological, and Atmospheric Studies: Technical Description and Users Guide*; Technical Note; Climate and Global Dynamics Division; National Center for Atmospheric Research: Boulder, CO, USA, 1996.
37. Friend, A.D. Parameterisation of a global daily weather generator for terrestrial ecosystem modelling. *Ecol. Model.* **1998**, *109*, 121–140. [[CrossRef](#)]
38. Liu, X.; Zhang, Y.; Han, W.; Tang, A.; Shen, J.; Cui, Z.; Vitousek, P.; Erisman, J.W.; Goulding, K.; Christie, P. Enhanced nitrogen deposition over China. *Nature* **2013**, *494*, 459–462. [[CrossRef](#)] [[PubMed](#)]
39. Rykiel, E.J. Testing ecological models: The meaning of validation. *Ecol. Model.* **1996**, *90*, 229–244. [[CrossRef](#)]
40. Jiang, C.; Wang, F.; Xing-Min, M.U.; Rui, L.I. Effects of temperature and precipitation variation on vegetation net primary productivity in the northern and southern regions of the qinling mountains from 1960 to 2011. *Acta Bot. Boreal.-Occident. Sin.* **2012**, *4*, 185–217.
41. ORNL DAAC. Available online: <http://daac.ornl.gov/> (accessed on 26 February 2017).
42. Wu, Y.; Wang, X.; Qiaoyan, L.I.; Yan, S. Response of broad-leaved Korean pine forest productivity of mt.Changbai to climate change: An analysis based on biome-bgc modeling. *Acta Sci. Nat. Univ. Pekin.* **2014**, *50*, 577–586.
43. Wang, Y. The Study of Soil Organic Carbon (N) Storage and Circulation Patterns in Ebinur Lake Wetland. Ph.D. Thesis, Xinjiang University, Xinjiang, China, 2015.
44. Su, H. Analyzing and Simulating the Growth of Picea Schrenkiana Forests in Xinjiang under Global Climate Change. Ph.D. Thesis, The Chinese Academy of Sciences, Beijing, China, 2005.
45. Pei, Z.Y.; Zhou, C.P.; Ouyang, H.; Yang, W.B. A carbon budget of alpine steppe area in the Tibetan Plateau. *Geogr. Res.* **2010**, *29*, 102–110.
46. Ying, W.; Tao, X.W.; Tian-gang, L.; Chao, W. Spacial and temporal dynamic changes of net primary product based on modis vegetation index in Gannan grassland. *Acta Pratacult. Sin.* **2010**, *19*, 201–210.
47. Walker, R.; Geisinger, D.; Johnson, D.; Ball, J. Elevated atmospheric CO<sub>2</sub> and soil n fertility effects on growth, mycorrhizal colonization, and xylem water potential of juvenile ponderosa pine in a field soil. *Plant Soil* **1997**, *195*, 25–36. [[CrossRef](#)]
48. Thomas, R.; Lewis, J.; Strain, B. Effects of leaf nutrient status on photosynthetic capacity in loblolly pine (*Pinus taeda* L.) seedlings grown in elevated atmospheric CO<sub>2</sub>. *Tree Physiol.* **1993**, *14*, 947–960. [[CrossRef](#)]
49. Kaushal, P.; Guehl, J.; Aussenac, G. Differential growth response to atmospheric carbon dioxide enrichment in seedlings of *Cedrus atlantica* and *Pinus nigra* ssp. *Laricio* var. *Corsicana*. *Can. J. For. Res.* **1989**, *19*, 1351–1358. [[CrossRef](#)]
50. Yang, B.; Wang, J.; Zhang, Y. Effect of long-term warming on growth and biomass allocation of abies faxoniana seedlings. *Acta Ecol. Sin.* **2010**, *30*, 5994–6000.
51. Bazzaz, F.; Coleman, J.; Morse, S. Growth responses of seven major co-occurring tree species of the northeastern United States to elevated CO<sub>2</sub>. *Can. J. For. Res.* **1990**, *20*, 1479–1484. [[CrossRef](#)]
52. Hui, Y.; Qian, W.; Jia, D.; Shouren, Z. Effects of precipitation and nitrogen addition on photosynthetically ecophysiological characteristics and biomass of four tree seedlings in Gutian mountain, Zhejiang province, China. *Acta Ecol. Sin.* **2013**, *33*, 4226–4236.
53. Smith, S.; Strain, B.; Sharkey, T. Effects of CO<sub>2</sub> enrichment on four great basin grasses. *Funct. Ecol.* **1987**, *1*, 139–143. [[CrossRef](#)]

54. Hunt, R.; Hand, D.; Hannah, M.; Neal, A. Response to CO<sub>2</sub> enrichment in 27 herbaceous species. *Funct. Ecol.* **1991**, *5*, 410–421. [[CrossRef](#)]
55. Gao, S.; Zhou, G. Response of stipa baicalensis to soil droughtstress at high CO<sub>2</sub> concentration. *J. Appl. Meteorol. Sci.* **2003**, *2*, 252–256.
56. Zhou, H.-K.; Zhou, X.-M.; Zhao, X.-Q. A preliminary study of the influence of simulated greenhouse effect on a kobresia humilis meadow. *Acta Phytoecol. Sin.* **2000**, *5*, 006.
57. Gao, S. *Effect of Warming and Nitrogen Addition on Structure and Function of Leymus Chinensis Community in Songnen Grassland*; Northeast Normal University: Changchun, China, 2012.
58. Li, Y.; Zhao, L.; Zhao, X.; Zhou, H. Effects of a 5-years mimic temperature increase to the structure and productivity of kobresia humilis meadow. *Acta Agrestia Sin.* **2003**, *12*, 236–239.
59. Li, F.; Zeng, X.D.; Song, X.; Tian, D.X.; Shao, P.; Zhang, D.L. Impact of spin-up forcing on vegetation states simulated by a dynamic global vegetation model coupled with a land surface model. *Adv. Atmos. Sci.* **2011**, *28*, 775–788. [[CrossRef](#)]
60. Wang, C.T.; Wang, Q.J.; Shen, Z.X.; Peng, H.C.; Hai ying, L.I. A preliminary study of the effect of simulated precipitation on an alpine kobresia humilis meadow. *Acta Pratacult. Sci.* **2003**, *12*, 25–29.
61. Housman, D.C.; Naumburg, E.; Huxman, T.E.; Charlet, T.N.; Nowak, R.S.; Smith, S.D. Increases in desert shrub productivity under elevated carbon dioxide vary with water availability. *Ecosystems* **2006**, *9*, 374–385. [[CrossRef](#)]
62. Polley, H.W.; Tischler, C.R.; Johnson, H.B. Elevated atmospheric CO<sub>2</sub> magnifies intra-specific variation in seedling growth of honey mesquite: An assessment of relative growth rates. *Rangel. Ecol. Manag.* **2006**, *59*, 128–134. [[CrossRef](#)]
63. Mauney, J.R.; Lewin, K.F.; Hendrey, G.R.; Kimball, B.A. Growth and yield of cotton exposed to free-air CO<sub>2</sub> enrichment (face). *Crit. Rev. Plant Sci.* **1992**, *11*, 213–222.
64. Kudo, G.; Suzuki, S. Warming effects on growth, production, and vegetation structure of alpine shrubs: A five-year experiment in northern Japan. *Oecologia* **2003**, *135*, 280–287. [[CrossRef](#)] [[PubMed](#)]
65. Xiao, C.; Zhang, X.; Zhao, J.; Wu, G. Response of seedlings of three dominant shrubs to climate warming to ordos plateau. *Acta Bot. Sin.* **2000**, *43*, 736–741.
66. Zhu, Y.-J.; Jia, Z.-Y.; Wu, B.; Lu, Q.; Yao, B. The role of increased precipitation in promoting branch and leaf growth of nitraria tangutorum. *For. Res.* **2012**, *5*, 016.
67. Chang, C.M. *Moisture Factor Dynamics and Its Impact on Aboveground Biomass in Stipa Klemenzii Steppe*; Inner Mongolia University: Inner Mongolia, China, 2014.
68. Zhang, C.; Lu, D.; Chen, X.; Zhang, Y.; Maisupova, B.; Tao, Y. The spatiotemporal patterns of vegetation coverage and biomass of the temperate deserts in central asia and their relationships with climate controls. *Remote Sens. Environ.* **2016**, *175*, 271–281. [[CrossRef](#)]
69. Hou, S.; Lei, L.; Zeng, Z. The response of global net primary productivity (npp) to CO<sub>2</sub> increasing and climate change: Evaluation of coupled model simulations. *J. Food Agric. Environ.* **2013**, *11*, 937–944.
70. Ahlström, A.; Raupach, M.R.; Schurgers, G.; Smith, B.; Arneeth, A.; Jung, M.; Reichstein, M.; Canadell, J.G.; Friedlingstein, P.; Jain, A.K. The dominant role of semi-arid ecosystems in the trend and variability of the land CO<sub>2</sub> sink. *Science* **2015**, *348*, 895–899. [[CrossRef](#)] [[PubMed](#)]
71. Marco, A.; David, M.; Hurtt, G.C.; Moorcroft, P.R. The contribution of land-use change, CO<sub>2</sub> fertilization and climate variability to the eastern US carbon sink. *Glob. Chang. Biol.* **2006**, *12*, 2370–2390.
72. Groenigen, K.J.V.; Qi, X.; Osenberg, C.W.; Luo, Y.; Hungate, B.A. Faster Decomposition under Increased Atmospheric CO<sub>2</sub> Limits Soil Carbon Storage. *Science* **2014**, *344*, 508–509. [[CrossRef](#)] [[PubMed](#)]
73. Liu, J.; Diamond, J. China's environment in a globalizing world. *Nature* **2005**, *435*, 1179–1186. [[CrossRef](#)] [[PubMed](#)]
74. Liu, Y.; Wang, D.; Gao, J.; Deng, W. Land use/cover changes, the environment and water resources in northeast China. *Environ. Manag.* **2005**, *36*, 691–701. [[CrossRef](#)] [[PubMed](#)]
75. Gao, J.; Liu, Y. Climate warming and land use change in heilongjiang province, northeast China. *Appl. Geogr.* **2011**, *31*, 476–482. [[CrossRef](#)]
76. Hu, Q.; Jiang, D.; Fan, G. Climate change projection on the tibetan plateau: Results of cmip5 models. *Chin. J. Atmos. Sci.* **2015**, *39*, 260–270.
77. Jinghong, Y.; Xu, L. The soil and water conservation and the utilization of rainfall resources in Inner Mongolia. In Proceedings of the 12th ISCO Conference, Beijing, China, 26–31 May 2002.

78. Shi, Y. Characteristics of late quaternary monsoonal glaciation on the tibetan plateau and in east Asia. *Quat. Int.* **2002**, *97*, 79–91. [[CrossRef](#)]
79. Naumburg, E.; Housman, D.C.; Huxman, T.E.; Charlet, T.N.; Loik, M.E.; Smith, S.D. Photosynthetic responses of mojave desert shrubs to free air CO<sub>2</sub> enrichment are greatest during wet years. *Glob. Chang. Biol.* **2003**, *9*, 276–285. [[CrossRef](#)]
80. Xu, H.; Li, Y.; Xu, G.; Zou, T. Ecophysiological response and morphological adjustment of two central asian desert shrubs towards variation in summer precipitation. *Plant Cell Environ.* **2007**, *30*, 399–409. [[CrossRef](#)] [[PubMed](#)]



© 2017 by the authors. Licensee MDPI, Basel, Switzerland. This article is an open access article distributed under the terms and conditions of the Creative Commons Attribution (CC BY) license (<http://creativecommons.org/licenses/by/4.0/>).